processes

MDPI

*Article*

# Optimization of Deep Learning Models for Enhanced Respiratory Signal Estimation Using Wearable Sensors

**Jiseon Kim [1] and Jooyong Kim [2,*]**

[1] Department of Smart Wearables Engineering, Soongsil University, Dongjak-gu, Seoul 06978, Republic of Korea
[2] Department of Material Science and Engineering, Soongsil University, Dongjak-gu, Seoul 06978, Republic of Korea
* Correspondence: jykim@ssu.ac.kr; Tel.: +82-2-820-0631

**Abstract:** Measuring breathing changes during exercise is crucial for healthcare applications. This study used wearable capacitive sensors to capture abdominal motion and extract breathing patterns. Data preprocessing methods included filtering and normalization, followed by feature extraction for classification. Despite the growing interest in respiratory monitoring, research on a deep learning-based analysis of breathing data remains limited. To address this research gap, we optimized CNN and ResNet through systematic hyperparameter tuning, enhancing classification accuracy and robustness. The optimized ResNet outperformed the CNN in accuracy (0.96 vs. 0.87) and precision for Class 4 (0.8 vs. 0.6), demonstrating its capability to capture complex breathing patterns. These findings highlight the importance of hyperparameter optimization in respiratory monitoring and suggest ResNet as a promising tool for real-time assessment in medical applications.

**Keywords:** deep learning; respiratory signal; wearable sensor; convolutional neural network; residual networks

check for updates

Academic Editors: Zhanxiao Kang and Qing Chen

Received: 22 January 2025
Revised: 17 February 2025
Accepted: 20 February 2025
Published: 4 March 2025

**Citation:** Kim, J.; Kim, J. Optimization of Deep Learning Models for Enhanced Respiratory Signal Estimation Using Wearable Sensors. *Processes* **2025**, *13*, 747. https://doi.org/10.3390/pr13030747

**Copyright:** © 2025 by the authors. Licensee MDPI, Basel, Switzerland. This article is an open access article distributed under the terms and conditions of the Creative Commons Attribution (CC BY) license (https://creativecommons.org/licenses/by/4.0/).

## 1. Introduction

Respiratory changes during exercise are critical indicators in healthcare fields, such as sports monitoring. Previous studies have suggested that fast inputs, including central command, primarily regulate respiratory signal during exercise [1]. This regulation may explain the strong association between respiratory signal and perceived exertion across various exercise conditions. Emerging evidence highlights that respiratory signal can effectively reflect the level of effort during cycling exercise [1–3]. In this way, respiratory signal serves as a prominent indicator of physical effort during exercise, surpassing the relevance of other commonly monitored physiological variables [4]. For example, respiration during exercise is primarily regulated by central command, along with input from muscle afferent fibers and metabolic signals [5]. Respiration is influenced by inputs that operate at distinct timings in response to sudden changes in exercise intensity. Rapid increases in respiration at the onset of exercise are driven by fast inputs, including central command and afferent feedback, while metabolic stimuli contribute to respiration with a delayed response [6]. Evidence indicates that respiratory signal more accurately represents physical effort compared to blood lactate, particularly in conditions such as post-exercise muscle damage [7], glycogen depletion [8], and in individuals with McArdle's disease [9]. Thus, respiratory signal provides corresponding data on physical effort during exercise.

Moreover, measuring respiratory signals is not an easy task, making wearable devices, data preprocessing, and analysis methods such as deep learning critical factors in the measurement process. Wearable devices come in a variety of forms, including clothing, bracelets,

and belts, each with their own advantages and disadvantages. Wearable respiratory sensors have gained significant attention for their ability to non-invasively monitor breathing patterns. Recent advancements, including deep learning-assisted portable biosensors, have enabled real-time respiratory analysis using compact and cost-effective devices [10]. Among these, clothing-based wearables are particularly well suited for everyday use. By utilizing lightweight and flexible materials, they allow for unrestricted movement, enabling the convenient measurement of body activity data, such as respiratory monitoring. For instance, a study developed a resistive sensor that can measure changes in breathing caused by emotional states. This was achieved by detecting changes in waist circumference, showing that clothing-based sensors can effectively capture respiratory changes associated with bodily movements [11]. Another study investigated textile-based sensors that measure breathing through contact resistance changes between fibers, even under different postural conditions [12]. Research on respiratory monitoring using clothing-based sensors is on the rise. However, while the classification of breathing patterns and data processing methods are critical, these aspects remain relatively underexplored.

Typically, respiratory signal estimation is directly performed from previously detected respiratory signals using deep learning, particularly Convolutional Neural Networks (CNNs) [13,14]. A CNN is a computational model composed of multiple processing layers capable of learning data representations [15]. This model enables tasks such as image classification, image segmentation, and action recognition. Despite their high applicability, CNNs occasionally encounter issues where neurons "die" during the learning process and fail to recover [16,17]. Additionally, as the model introduces more parameters, overfitting may occur, or training errors may increase [18]. To overcome these challenges, various methods have been proposed, one of which involves using a Residual Network (ResNet) [19,20]. Deep learning is utilized not only in medical image analysis but also in the classification of bio signals using wearable sensors, making it particularly useful for processing time series such as breathing patterns [21]. The key distinction of ResNet lies in the inclusion of shortcut connections within convolutional layers. These connections help address common CNN issues, allowing the gradient to backpropagate more effectively, thereby accelerating the training process [22]. As demonstrated, different training methods have distinct characteristics, and selecting the appropriate deep learning model that aligns with the research objective is essential. Additionally, choosing suitable parameters based on the characteristics of the data can significantly impact the accuracy of the results. Therefore, the selection of an appropriate deep learning model and parameter configuration that fit the research objective is crucial.

In this study, respiratory data generated during physical activity were trained using deep learning models such as CNN and ResNet to identify the most suitable approach for improving prediction accuracy. To measure respiration during exercise, a wearable respiration sensor was developed. The sensor was designed to be positioned at the front and back of the torso, specifically near the xiphoid process, to measure changes in capacitance caused by thoracic expansion and contraction during breathing. The respiration changes were observed according to different exercise conditions. To accurately classify and detect these changes, a comparative analysis of CNN and ResNet models was conducted. The method that demonstrated higher accuracy was considered the most appropriate for the given dataset. These findings highlight the development of an optimized system for selecting deep learning models that best suit the characteristics and objectives of the dataset, ultimately enhancing prediction accuracy. The research process is illustrated in Figure 1, providing a clear visualization of the study's workflow. This diagram helps readers easily understand the research objectives.

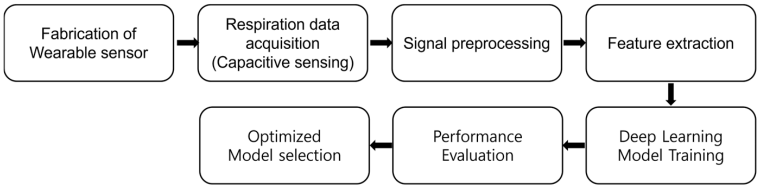



**Figure 1.** A schematic of the proposed work.

## 2. Materials and Methods

### *2.1. Respiration Measurement System*

#### 2.1.1. Breathing Mechanism

Understanding the mechanism of breathing is essential for accurate respiratory measurement. Equally important is the selection of a sensor measurement method that effectively corresponds to this mechanism. Various methods exist for measuring respiration, including monitoring airflow through the nose, capturing respiratory sounds, and tracking abdominal movement. Among these, this study focuses on measuring abdominal movement. This approach was chosen because it is the most suitable for wearable sensor applications and can be easily implemented in daily life.

In this method, respiration is measured using capacitive values $(C)$ derived from abdominal movement (Equation (1)). The principle of measurement is as follows: when inhaling, air enters the lungs, causing the lungs to expand. This expansion leads to the spreading of the ribcage and the subsequent expansion of the thorax and abdomen. Conversely, when exhaling, air exits the lungs, the ribcage contracts, and the abdomen compresses. This process results in variations in abdominal volume, which correspond to changes in the distance between electrodes in a capacitive sensing system. By analyzing these differences in capacitive values, respiration can be assessed.

The two sensors were placed on the front and back of the body near the xiphoid process, where the abdominal movements caused by breathing can be most effectively measured. When the abdomen expands, the distance between the electrodes $(d)$ is denoted as $d_0$, and during contraction, it is $d_f$. The difference between these distances, $\Delta d$, is used to analyze respiration (Equation (2)). The measurement principle and the breathing mechanism are illustrated in Figure 2 [23].

$$C = \frac{\varepsilon A}{d} \tag{1}$$

$$\Delta d = d_f - d_0 \tag{2}$$

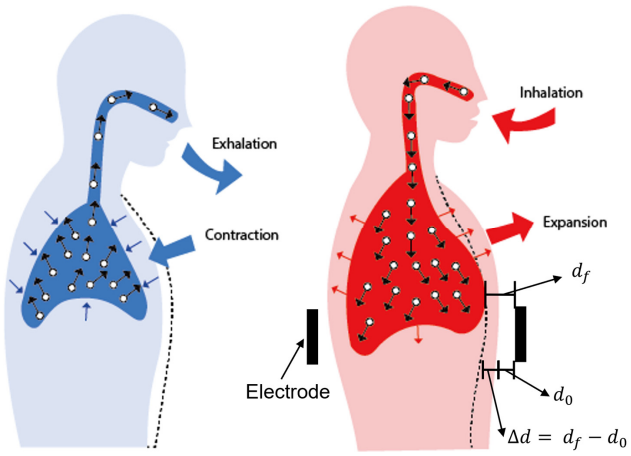



**Figure 2.** Abdominal movement in response to breathing [23].

2.1.2. Fabrication of Wearable Sensors

The electrodes were designed to have a rectangular shape with dimensions of 100 mm in width and 50 mm in height. The connectors for measurement were circular, measuring 20 mm × 20 mm. The stitch connecting the sensors to the connector was made in a zigzag pattern with a total length of 335 mm. The placement of the sensors is shown in Figure 3a, where the distances relative to reference points can also be observed. The area density of the embroidery (line/mm) was set to 6 for the sensor electrodes and 4.5 for the connectors. As the connection line consists of stitch lines, it does not have an embroidery area density. Regarding the stitch pattern, the electrodes and connectors were designed with a running stitch for the top thread and a fill stitch for the bobbin thread, while the connection line used a zigzag stitch.

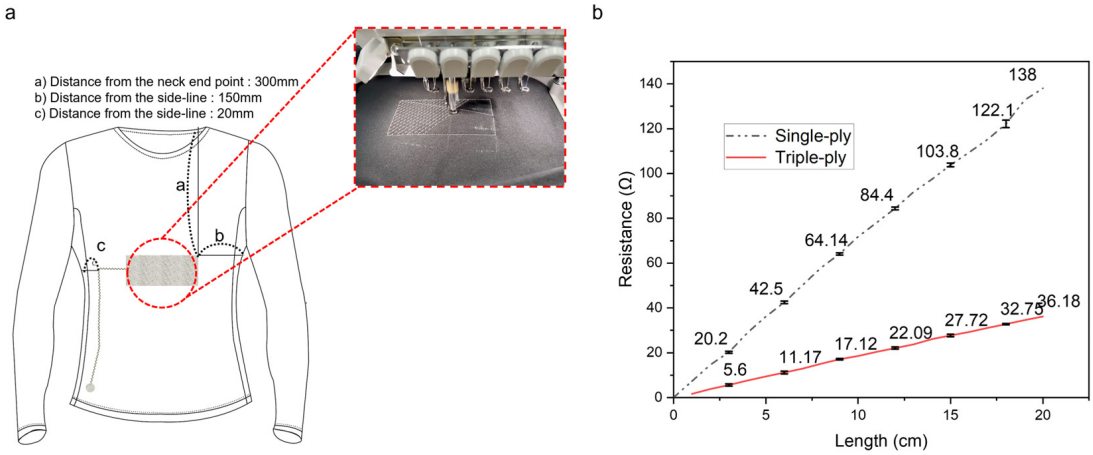



**Figure 3.** (**a**) Wearable sensors in the shape of a finished garment [23]; (**b**) the effect of single-ply and triple-ply thread length on the resistance value.

The stitch length for the electrodes and connectors was set to a width of 2 mm and a height of 4 mm, whereas the connection line had a width of 5 mm and a height of 1 mm. Finally, the total amount of thread used was 9526 stitches for the electrodes and 606 stitches for the connectors. This information is provided only for embroidered area measurements. Detailed specifications of the sensors are provided in Table 1 [24].

**Table 1.** Specifications of the wearable sensors.

| Parameter | Electrodes | Connection Line | Connectors |
|---|---|---|---|
| Dimension (width × height) | 100 × 50 ($mm^2$) | 335 ($mm^2$) | 20 × 20 ($mm^2$) |
| Density (line/mm) | 6 | - | 4.5 |
| Shape of stitch | Running, fill | Zigzag | Running, fill |
| Length of stitch (mm) | 2, 4 | 5/1 (width/height) | 2, 4 |
| Number of stitches | 9526 | - | 606 |

The electrodes of the sensors were directly embroidered onto fabric (87% polyester, 13% spandex) (Sumnfit, Seoul, Republic of Korea) using silver-coated thread (AMANN, Bönnigheim, Germany) and an embroidery machine (BROTHER, Bridgewater, NJ, USA). Silver-coated thread was used as the top thread, while 100% rayon embroidery thread was used as the bobbin thread. The top thread was placed on the inner side of the garment, which encounters the body, while the bobbin thread remained on the outer side. To protect the outer side, a polyurethane (PU) film was heat-bonded onto the surface.

As shown in Figure 3a [23], rectangular electrodes were directly embroidered onto the front and back of the garment near the xiphoid process. The electrode placement was chosen to align with the areas of the abdomen that exhibit the most significant volume changes during respiration. To prevent any obstruction to breathing during measurements, the connector was positioned at the bottom hem of the garment, allowing seamless connection to the measurement device. The connectors were symmetrically aligned on both the front and back of the garment. To connect the electrodes and the connectors, a zigzag stitch was used, creating a straight pathway from the rectangular electrodes to the circular connectors.

The silver-coated thread consists of 34 twisted nylon filaments. This thread is widely used in wearable applications due to its compatibility with embroidery [25] and sewing machines. It has also been evaluated as safe in cytotoxicity tests following the biological evaluation standard for medical devices (DIN EN ISO 10993-5) [26]. Therefore, it is suitable for placement on the inner side of garments where it comes into direct contact with the skin. In this regard, ply refers to the unit indicating the number of strands twisted together to form a thread. A single-ply thread consists of one twisted strand, while a triple-ply thread consists of three twisted strands. As shown in Figure 3b [27], the resistance of the thread decreases as the number of twists increases, demonstrating that the thread used in this study minimizes measurement errors caused by resistance.

### *2.2. Experimental Setup and Acquistion*

The experiment was conducted to measure breathing under different intensity levels through cycling. The measurement process involved wearing a garment-based sensor and using an indoor cycling apparatus (XAMEN KANGTO FITNESS FOUPWENT CO, Xiamen, China). For precise measurements, an LCR meter (KEYSIGHT, Santa rosa, CA, USA) and the Keysight Benchvue program (KEYSIGHT, Santa Rosa, CA, USA) were employed instead of simple devices.

The intensity levels were divided into four categories: resting state (no activity), low intensity, moderate intensity, and high intensity. Low intensity corresponded to an average speed of 15–20 km/h, moderate intensity to 20–30 km/h, and high intensity to 30–40 km/h. Each intensity level was measured for 5 min, followed by a 1 min rest period before proceeding to the next measurement. The schematic diagram of the measurement setup is shown in Figure 4a [23], and the actual measurement process is illustrated in Figure 4b. The temperature was measured at room temperature (18 °C to 20 °C), and the experiment was conducted at approximately 60% humidity.

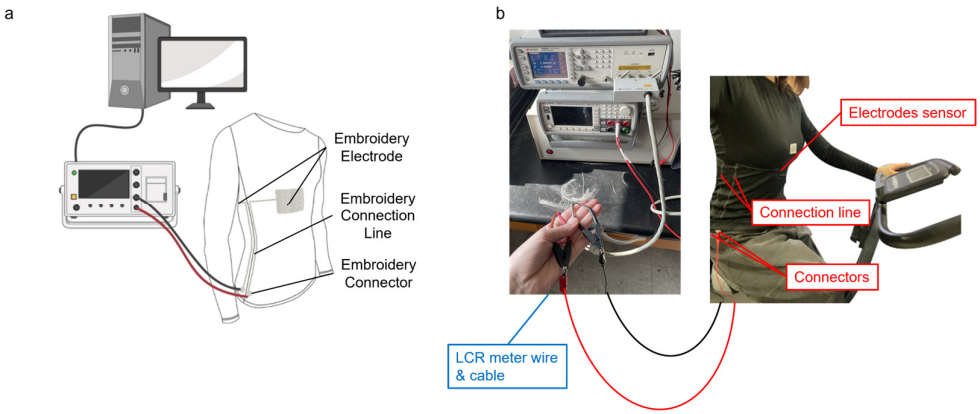



**Figure 4.** (**a**) Schematic of LCR meter [23]; (**b**) measurement of wearable sensors.

### *2.3. Signal Processing with Deep Learning*

Signal processing was conducted using MATLAB R2023a. The data, representing the capacitive values of the sensor corresponding to respiration, were normalized to a range between −3 and 3 to enhance model generalization and improve training stability. Using the normalized data, classification results were analyzed with CNN and ResNet to determine the most suitable algorithm for the dataset used in this study. Figure 5 illustrates the hierarchical structures of the networks, where 5a represents the CNN architecture and 5b depicts the ResNet architecture.

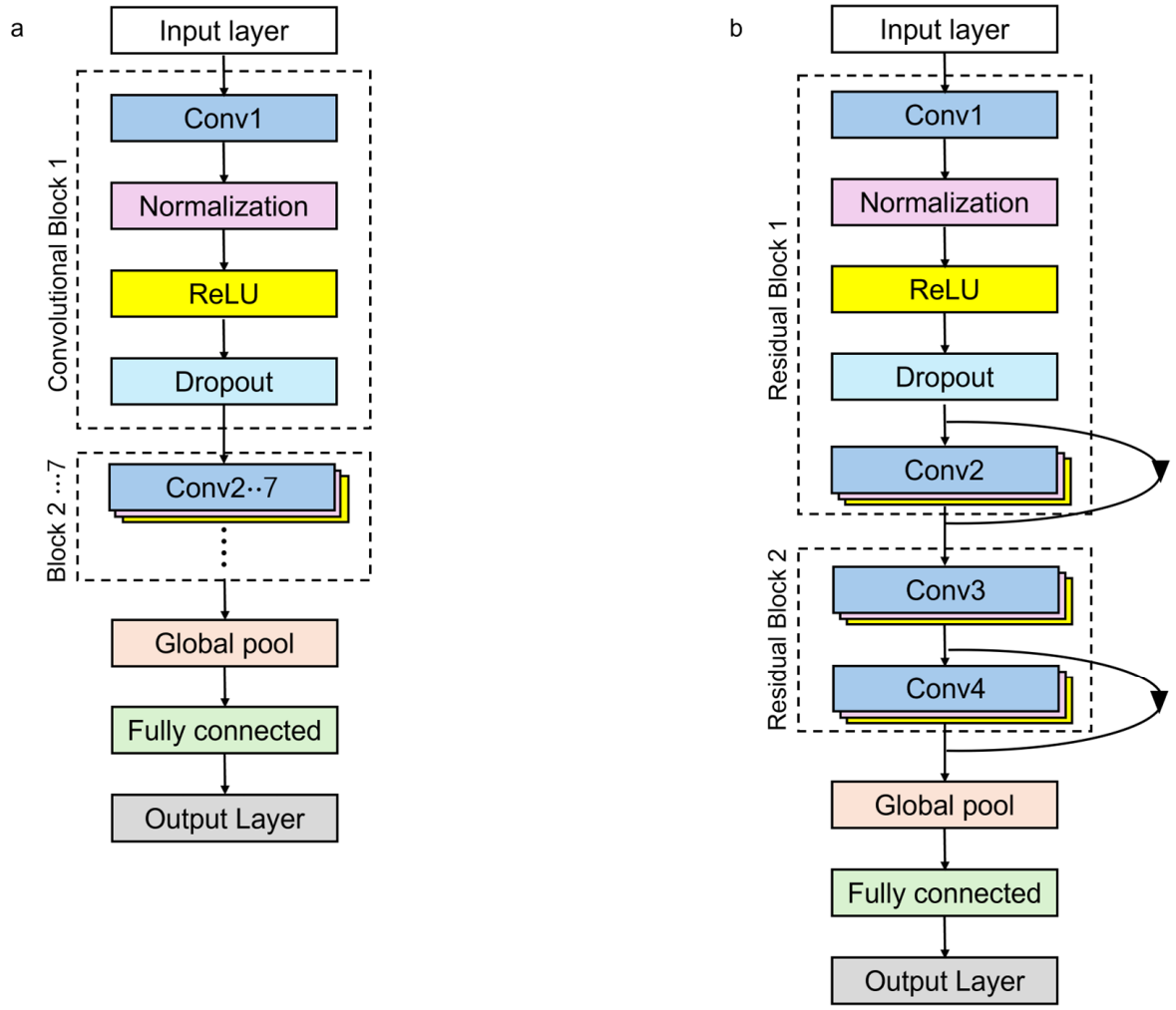



**Figure 5.** (**a**) CNN architecture; (**b**) ResNet architecture.

A CNN is an algorithm that processes multiple layers sequentially. The CNN used in this study consists of seven convolutional blocks, each containing convolution, normalization, ReLU, and dropout layers. After repeating these blocks seven times, the network concludes with a global pooling layer and a fully connected layer for final classification. Through the pooling layer, features can be directly extracted, and hierarchical learning makes it effective for capturing complex data. However, as mentioned in the introduction, issues such as neuron death and non-recovery occasionally occur during this process. To address these limitations, ResNet, which has a similar structure but overcomes such challenges, is one of the alternative algorithms.

The structure of ResNet consists of two residual blocks, each containing two sets of convolutional blocks. A distinguishing feature of ResNet is its ability to learn the

residual function $F(x)$, which represents the difference between the input $(x)$ and the output $(y)$, unlike conventional neural networks. The mathematical representation of the residual function is provided in Equation (3), where $H(x)$ denotes the target function. Furthermore, as illustrated in Figure 5b, simple skip connections ensure that information is preserved during transmission, preventing performance degradation even as the network depth increases. The mathematical formulation of these skip connections can be found in Equation (4). After the residual blocks, the network concludes with global pooling and a fully connected layer, like CNN, to produce the final classification results.

$$F(x) = H(x) - x \tag{3}$$

$$y = F(x) + x \tag{4}$$

The total dataset consists of 157 samples, with 100 sets used for training, 24 sets for validation, and 23 sets for testing. Both algorithms classify four classes using a single input. The dropout rate is set at 0.5, with a filter size of 5 and 32 filters. The maximum number of epochs is configured as 200 for CNN and 1000 for ResNet. The initial learning rate is set to 0.0005 for CNN and 0.001 for ResNet.

Table 2 includes all materials and methods used in this work together with their purposes.

**Table 2.** Summary of analyzed materials and test devices used.

| Component | Remark | Manufacture | Purpose |
|---|---|---|---|
| Electrodes | Silver-coated outer nylon cores covered by PU | AMANN, Bönnigheim, Germany | Creating sensing area of upper and lower plates |
| Embroidery machine | PR670E | BROTHER, Bridgewater, NJ, USA | Sewing electrodes, connection wires, and connectors |
| Indoor cycling apparatus | MKHB-01 | XAMEN KANGTO FITNESS FOUPWENT CO, Xiamen, China | Device for measuring respiration based on exercise intensity |
| LCR meter | E4980AL | KEYSIGHT, Santa rosa, CA, USA | Measurement of capacitance values based on respiration |
| MATLAB | R2023a | MathWorks, Natick, MA, USA | Data classification and optimization using deep learning |

## 3. Results and Discussion

Breathing data were collected under four conditions, resting, low intensity, moderate intensity, and high intensity, based on changes in cycling speed. Using this dataset, classification was performed using both CNN and ResNet algorithms, and their results were compared to determine the most suitable algorithm for this classification task. Figure 6 sequentially presents the capacitive data measured by the respiratory sensor for each condition: (a) resting, (b) low intensity, (c) moderate intensity, and (d) high intensity. Additionally, the results were derived by comparing accuracy, precision, recall, and the F1-score. Accuracy refers to the proportion of correctly predicted samples out of the total samples. Precision measures the proportion of true positive predictions among all positive predictions, while recall measures the proportion of true positive instances among all actual positive instances. The F1-score represents the harmonic meaning of precision and recall.

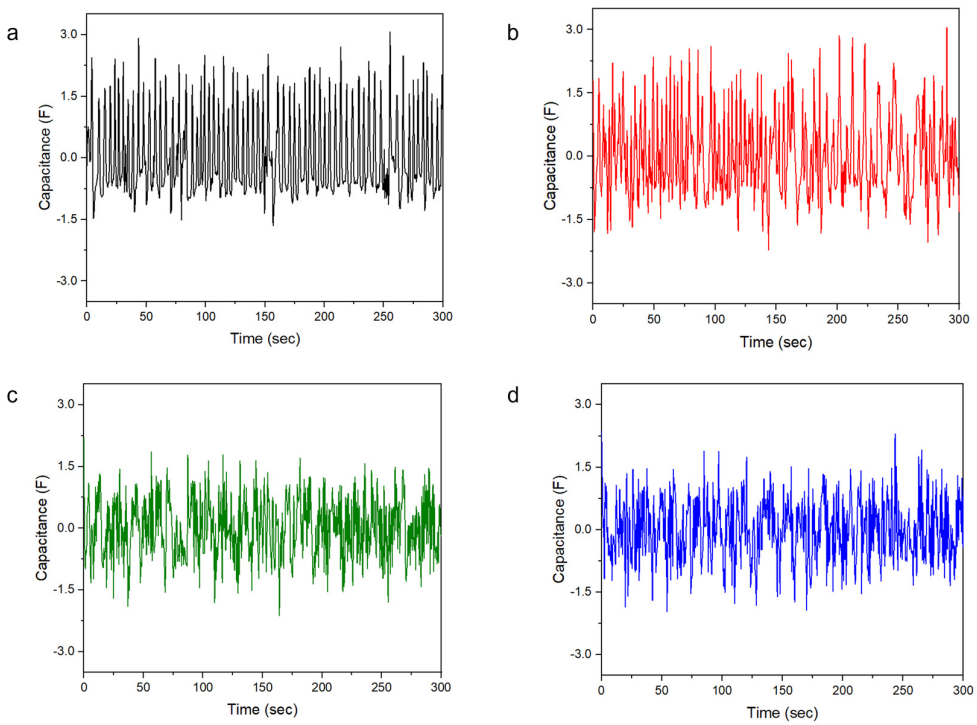



**Figure 6.** Breathing data under different conditions: (**a**) resting; (**b**) low intensity; (**c**) moderate intensity; and (**d**) high intensity.

### *3.1. Analysis of Results from CNN Algorithms*

During the process of result derivation, the parameters and the number of blocks were adjusted to identify the most suitable configuration. In the initial model, CNN-1, the baseline number of blocks was set to seven, with the hypothesis that increasing the number of blocks would enhance training capacity and ultimately improve final accuracy. Deep learning training was conducted under this assumption.

Contrary to expectations, the training results failed to identify meaningful patterns, resulting in significantly low validation and test accuracy of 25%. Instead, all predictions were classified as resting (Class 1) breathing. These outcomes are visualized in Figure 7, where (a) displays the training results window, and (b) presents the confusion matrix.

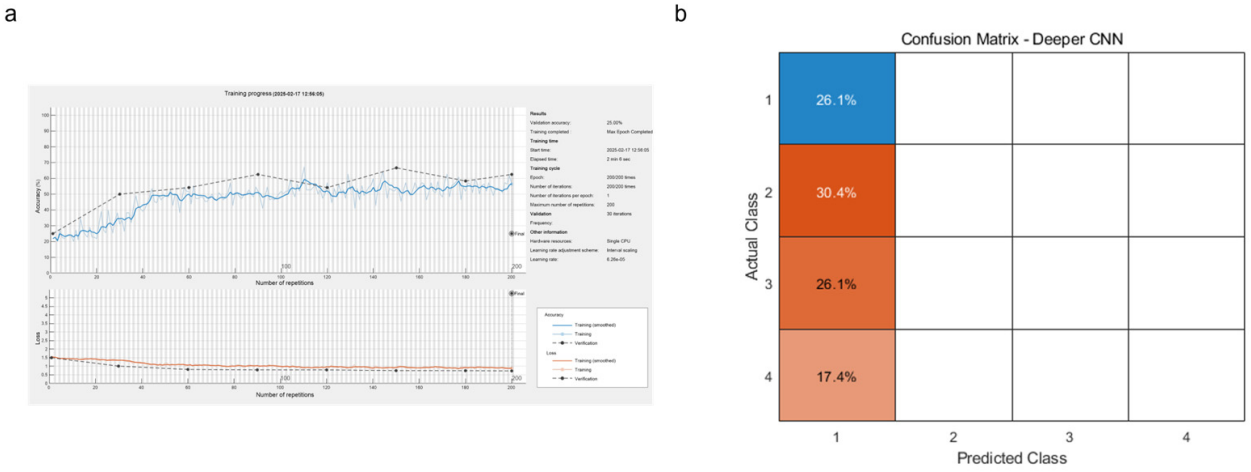



**Figure 7.** (**a**) Training results window; (**b**) confusion matrix (CNN-1).

This result suggests that increasing the number of blocks led to overfitting, thereby degrading generalization performance. Additionally, it may be attributed to information loss during propagation due to neuron deletion, which was previously identified as an issue.

In the second training session (O-CNN), improvements were made by fixing the number of blocks at seven and varying the number of epochs between 150 and 300 to identify the point where accuracy steadily increased without overfitting. Ultimately, the most stable gradient was achieved at 200 epochs. The final validation accuracy reached 79.16%, while the test accuracy was 83.92%. Additionally, the final loss value decreased to 0.89. Therefore, this model represents the optimized CNN (O-CNN) configuration, and the validation accuracy results along with the final loss value graph are shown in Figure 8a,b, respectively. These findings suggest that a deeper network than the CNN classification algorithm and an approach capable of preserving information throughout propagation are required to achieve the optimal outcome for this dataset.

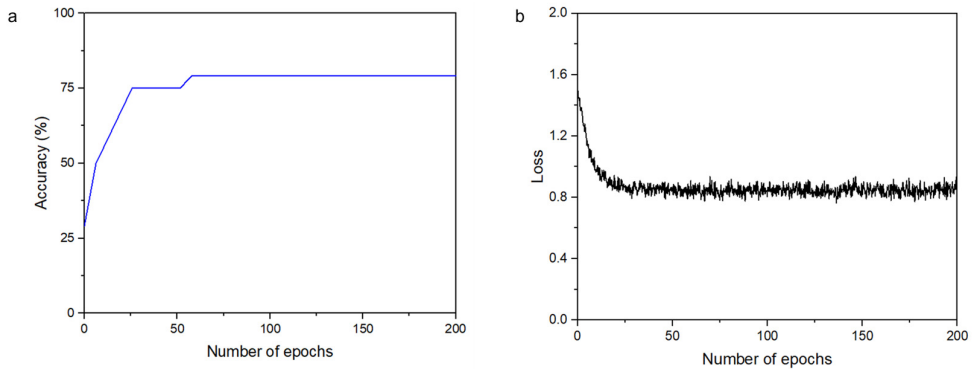



**Figure 8.** The results of O-CNN. (**a**) Validation accuracy; (**b**) training loss.

### *3.2. Analysis of Results from ResNet Algorithms*

Training with ResNet also involved varying the number of epochs to test for accurate improvements. Compared to CNN, ResNet utilizes a deeper network, requiring a longer training duration to achieve higher accuracy. Accordingly, the training was conducted with epochs ranging from 1000 to 2000, with the initial training set to approximately 2000 epochs. Unlike CNN, ResNet demonstrated superior initial performance, achieving a validation accuracy of 87.5% and a notably low loss value of 0.4. Both the testing and validation curves showed similar trends with gradual gradients. The test accuracy reached an impressive 91%. These results indicate that ResNet effectively overcomes the limitations of CNN by leveraging skip connections to mitigate neuron loss, leading to higher accuracy. The results are illustrated in Figure 9a,b.

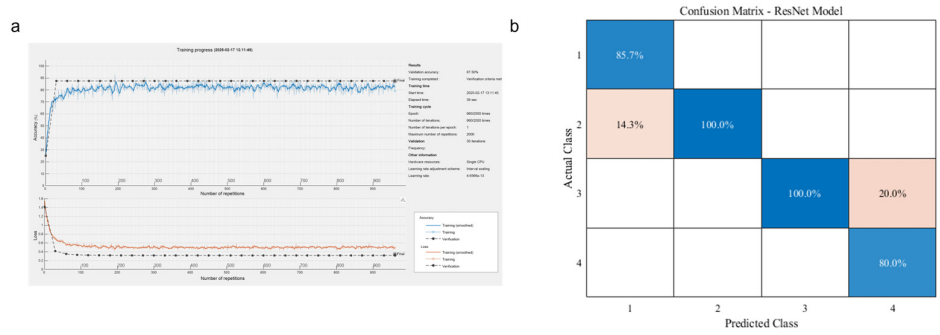



**Figure 9.** (**a**) Training results window; (**b**) confusion matrix (ResNet-1).

The test results were further improved when we used the optimized ResNet (O-ResNet), with the number of epochs reduced to 1000 for retraining. While the validation accuracy remained similar at 87%, the loss value decreased significantly to 0.003, and the test accuracy increased to 95%. These results suggest that an excessive number of epochs can negatively impact test performance and confirm that ResNet is more suitable for classifying this dataset compared to CNN. These results can be observed in Figure 10.

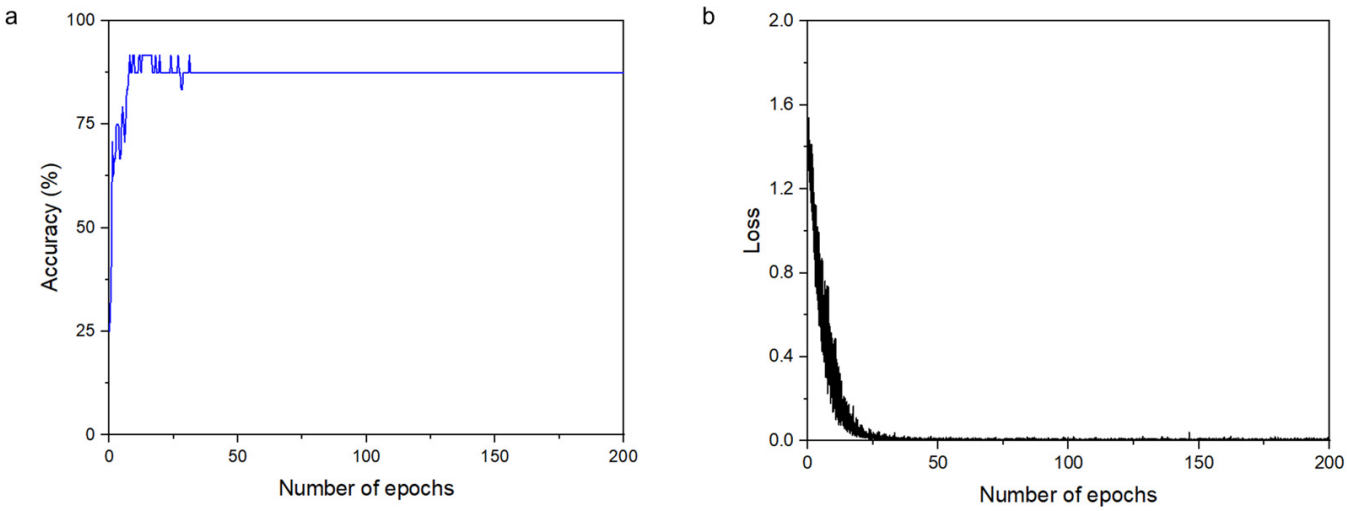



**Figure 10.** The results of O-Resnet. (**a**) Validation accuracy; (**b**) training loss.

The comparative analysis of CNN and ResNet in this study highlights the effectiveness of deep learning architectures in respiratory signal classification. While both models share similar layer structures, ResNet's skip connections play a crucial role in preserving important features during training, thereby enhancing classification performance. The ability of ResNet to maintain higher accuracy across different training conditions underscores the importance of selecting appropriate network structures and training parameters. These findings demonstrate that deep learning model selection and optimization are critical factors in achieving robust classification performance for physiological signal processing.

### *3.3. A Comparison to the State of the Art*

The proposed models' performance is presented in comparison with existing deep learning-based studies on similar datasets, as shown in Table 3. The results indicate that the optimized CNN (O-CNN) model achieved an accuracy of 83.92%, while the optimized ResNet (O-ResNet) model attained an accuracy of 95%. Although our models did not surpass all previously published studies, they demonstrated performance comparable to the highest accuracy levels reported in the literature.

A review of related research reveals that many studies focus on combining models optimized for specific datasets or conducting comparative analyses with existing architectures. However, there remains a lack of studies exploring parameter tuning experiments and the application of deep learning to respiratory signal-based data analysis. These findings highlight the necessity of this research and underscore the importance of optimizing deep learning models for specific datasets.

While our models did not achieve the highest reported accuracy, they successfully reached the performance range of state-of-the-art studies. More importantly, this study contributes to the field by identifying dataset-specific optimal models through adjustments in the number of epochs and network blocks, demonstrating the significance of tailored optimization in deep learning applications.

**Table 3.** A comparison with state-of-the-art deep learning models.

| Authors | Model | Accuracy (%) |
|---|---|---|
| [28] | Convolutional Neural Network—Mixture of Experts (CNN-MoE) | 84.6 |
| [29] | Deep Convolutional Autoencoder (CAE) | 94.2 |
| [30] | Convolutional Autoencoder for Multi-Person Activity Sensing (CAE-MAS) | 97.13 |
| [31] | Artificial Hydrocarbon Network (ANN) | 98.24 |
| [19] | ResNet-18, ResNet-34, ResNet-50, ResNet-101, ResNet-152 | 96.43 |
| [32] | Convolutional Neural Network (CNN) | 94.5 |
| [33] | Residual Neural Network (ResNet) | 99.99 |
| [20] | ResNet-RS (Improved ResNet Scaling Strategies) | 86.2 |
| | Optimized Convolutional Neural Network (O-CNN) | 83.92 |
| | Optimized Residual Neural Network (O-ResNet) | 95 |

### *3.4. Classification Analysis Across Different Breathing Intensities*

The classification of the four types of breathing was analyzed based on accuracy, precision, recall, and F1-score to evaluate how well each breathing type was classified. The results of the classification using O-CNN are presented in a confusion matrix, as shown in Figure 11. The four classes are as follows: Class 1 represents resting, Class 2 represents low-intensity breathing, Class 3 represents moderate-intensity breathing, and Class 4 represents high-intensity breathing.

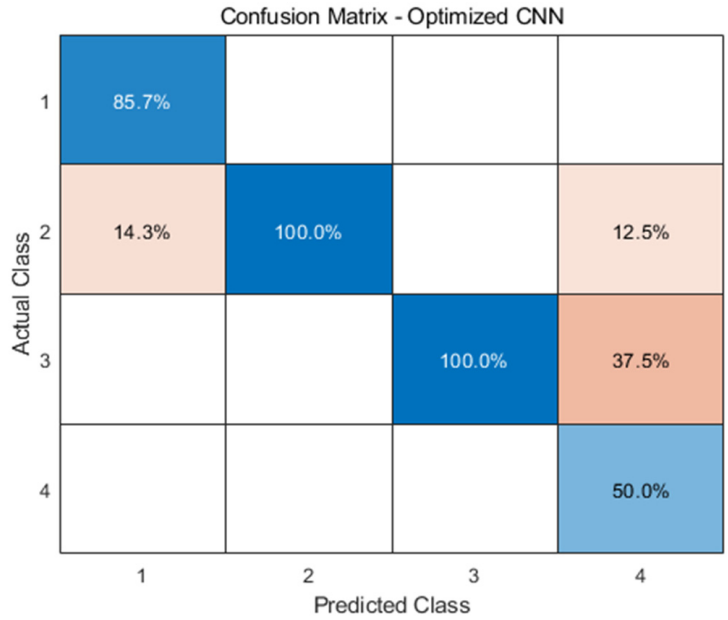



**Figure 11.** Confusion matrix of O-CNN.

The accuracy of the model is observed by examining the true positive (TP) values along the diagonal of the confusion matrix, with an overall accuracy of 0.87. The precision values for each class are 1.0, 0.85, 1.0, and 0.6, respectively. Similarly, the recall values for the classes are 0.83, 1.0, 0.75, and 1.0. Finally, the F1-scores for the classes are 0.9, 0.92, 0.86, and 0.75, in the same order. Both precision and recall values above 0.7 are generally considered satisfactory. Based on these results, the O-CNN metrics demonstrate satisfactory performance overall. However, for Class 4, the precision is significantly low at 0.6, indicating reduced reliability in classification. Additionally, the F1-score for Class 4 is also relatively low at 0.75, suggesting that O-CNN performs the least effectively for this specific class. The detailed metrics can be found in Table 4.

**Table 4.** Classification performance metrics of O-CNN.

| Metric | Class 1 | Class 2 | Class 3 | Class 4 | Macro Average |
|---|---|---|---|---|---|
| Precision | 1.0 | 0.85 | 1.0 | 0.6 | 0.86 |
| Recall | 0.83 | 1.0 | 0.75 | 1.0 | 0.9 |
| F1-score | 0.9 | 0.92 | 0.86 | 0.75 | 0.86 |
| Accuracy | | | | | 0.87 |

The results of the O-ResNet classification showed an accuracy of 0.95. The precision values were as follows: 1.0 for Class 1, 1.0 for Class 2, 1.0 for Class 3, and 0.8 for Class 4. The recall values were 1.0, 0.86, 1.0, and 1.0, respectively. Finally, the F1-scores were 1.0 for Class 1, 0.92 for Class 2, 1.0 for Class 3, and 0.89 for Class 4. These results indicate strong overall performance, with all metrics exceeding 0.7, which is generally considered a good threshold.

A detailed analysis revealed the following:

Class 1 achieved a perfect score (1.0) across all metrics, demonstrating that O-ResNet enables flawless classification for this category.

Class 2 showed a slightly lower recall compared to precision, indicating a minor shortfall in correctly predicting actual positive instances from the dataset.

Class 3 exhibited perfect scores across all metrics, confirming its reliable classification.

Class 4 had the lowest precision (0.8) among all metrics. As shown in the confusion matrix (Figure 12), while all other classes were classified with 100% accuracy, Class 4 was classified with an 80% accuracy rate. Nevertheless, since all metrics exceed 0.7, this is considered satisfactory. When precision and recall were harmonically averaged, Class 4 achieved an F1-score of 0.89, which is close to 1.

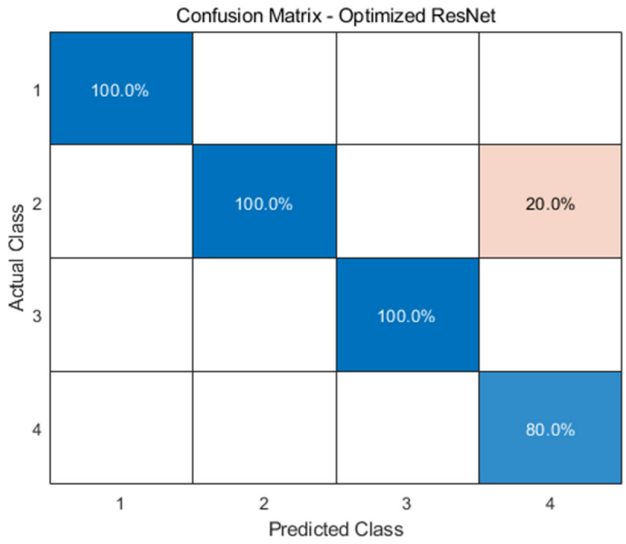



**Figure 12.** Confusion matrix of O-ResNet.

These results demonstrate that O-ResNet classification is well suited for this dataset, particularly as indicated by the F1-score, which accounts for both precision and recall. Furthermore, the results reflect the strong performance of the O-ResNet model, indicating appropriate parameter selection and effective use of the data. All evaluation metrics are summarized in Table 5.

To further assess the effectiveness of the O-ResNet model, its performance was compared to that of O-CNN using standard deep learning evaluation metrics. Accuracy, precision, recall, and the overall F1-score were used for comparison, and the results were analyzed for each breathing intensity. When comparing accuracy, O-CNN achieved 0.87,

while O-ResNet achieved 0.96, both of which are considered satisfactory. A closer examination of the metrics revealed that the precision for Class 4 was 0.6 in O-CNN but significantly improved to 0.8 in O-ResNet. These findings indicate that O-ResNet enhances precision and demonstrates its suitability and reliability for the classification task in this study.

**Table 5.** Classification performance metrics of O-ResNet.

| Metric | Class 1 | Class 2 | Class 3 | Class 4 | Macro Average |
|---|---|---|---|---|---|
| Precision | 1.0 | 1.0 | 1.0 | 0.8 | 0.95 |
| Recall | 1.0 | 0.86 | 1.0 | 1.0 | 0.96 |
| F1-score | 1.0 | 0.92 | 1.0 | 0.89 | 0.95 |
| Accuracy | | | | | 0.96 |

In this study, a wearable respiratory sensor was employed to classify breathing patterns of varying intensities across cycles using deep learning techniques. The results demonstrate that wearable respiratory sensors can effectively capture and differentiate breathing patterns in both physical activities and daily life. The enhanced classification performance of O-ResNet highlights its potential for detecting abnormal breathing patterns, which could be valuable for health monitoring applications.

Despite these promising results, several challenges remain. First, the dataset used in this study was relatively small and was collected under controlled conditions, which may limit its generalizability. Future research will address this limitation by incorporating a more diverse dataset, considering various exercise conditions, postures, and sensor placements. Second, while O-ResNet demonstrated strong performance, it may encounter difficulties in processing more complex breathing patterns or real-time applications. To overcome these challenges, future work will explore alternative models, such as LSTM or GAN, which may enhance classification accuracy, particularly for long-term respiratory monitoring and data augmentation. Lastly, the real-world implementation of wearable respiratory sensors requires careful consideration of factors such as sensor placement variability, motion artifacts, and individual differences. Future studies will focus on refining sensor design and preprocessing techniques to improve the practicality of these models in real-world health monitoring systems.

## 4. Conclusions

This study investigated the classification of breathing patterns using a wearable respiratory sensor and deep learning models. The findings confirm that O-ResNet, with its skip connection architecture, outperformed O-CNN in accuracy and precision, particularly in detecting high-intensity breathing patterns. These results underscore the potential of wearable sensors and deep learning techniques for real-time health monitoring, offering a promising approach for capturing complex respiratory signals.

Despite these advancements, this study has limitations, including the relatively small dataset collected under controlled conditions. To address this, future research should incorporate larger and more diverse datasets while also exploring alternative models, such as LSTM or GAN, to improve classification performance. The insights gained from this study contribute to the advancement of wearable respiratory monitoring, paving the way for more accurate and reliable health applications.

**Author Contributions:** As a corresponding author, J.K. (Jooyong Kim) was responsible for the entire structure's construction, while J.K. (Jiseon Kim) was responsible for the experimental design and modeling. J.K. (Jiseon Kim) was responsible for data collection, data processing, and material selection. J.K. (Jooyong Kim) and J.K. (Jiseon Kim) drafted the manuscript. All authors have read and agreed to the published version of the manuscript.

**Funding:** This research was financially supported by Soongsil University, Seoul 156-743, Republic of Korea. This work was supported by the Technology Innovation Program (Industrial Strategic Technology Development Program: Materials/Parts Package Type, grant number 20016038; Development of textile–IT converged digital sensor modules for smart wear to monitor bio and activity signals in exercise and KS standard), the Ministry of Trade, Industry and Energy (MOTIE, Republic of Korea), and the Korea Institute for Advancement of Technology (KIAT, MOTIE), grant number P0012770 (The Competency Development Program for Industry Specialist).

**Data Availability Statement:** The original contributions presented in this study are included in the article; further inquiries can be directed to the corresponding authors.

**Conflicts of Interest:** The authors declare no conflicts of interest.

## References

1. Nicolò, A.; Marcora, S.M.; Bazzucchi, I.; Sacchetti, M. Differential control of respiratory frequency and tidal volume during high-intensity interval training. *Exp. Physiol.* **2017**, *102*, 934–949. [CrossRef]
2. Nicolò, A.; Bazzucchi, I.; Haxhi, J.; Felici, F.; Sacchetti, M. Comparing continuous and intermittent exercise: An "isoeffort" and "isotime" approach. *PLoS ONE* **2014**, *9*, e94990. [CrossRef]
3. Nicolò, A.; Marcora, S.M.; Sacchetti, M. Respiratory frequency is strongly associated with perceived exertion during time trials of different duration. *J. Sports Sci.* **2016**, *34*, 1199–1206. [CrossRef]
4. Nicolò, A.; Massaroni, C.; Passfield, L. Respiratory frequency during exercise: The neglected physiological measure. *Front. Physiol.* **2017**, *8*, 922. [CrossRef]
5. Forster, H.V.; Haouzi, P.; Dempsey, J.A. Control of breathing during exercise. *Compr. Physiol.* **2011**, *2*, 743–777.
6. Duffin, J. The fast exercise drive to breathe. *J. Physiol.* **2014**, *592*, 445–451. [CrossRef] [PubMed]
7. Davies, R.C.; Rowlands, A.V.; Poole, D.C.; Jones, A.M.; Eston, R.G. Eccentric exercise-induced muscle damage dissociates the lactate and gas exchange thresholds. *J. Sports Sci.* **2011**, *29*, 181–189. [CrossRef]
8. Busse, M.; Maassen, N.; Konrad, H. Relation between plasma K+ and ventilation during incremental exercise after glycogen depletion and repletion in man. *J. Physiol.* **1991**, *443*, 469–476. [CrossRef]
9. Voduc, N.; Webb, K.A.; D'Arsigny, C.; McBride, I.; O'Donnell, D.E. McArdle's Disease Presenting as Unexplained Dyspnea in a Young Woman. *Can. Respir. J.* **2004**, *11*, 163–167. [CrossRef] [PubMed]
10. Bhaiyya, M.; Rewatkar, P.; Pimpalkar, A.; Jain, D.; Srivastava, S.K.; Zalke, J.; Kalambe, J.; Balpande, S.; Kale, P.; Kalantri, Y. Deep Learning-Assisted Smartphone-Based Electrochemiluminescence Visual Monitoring Biosensor: A Fully Integrated Portable Platform. *Micromachines* **2024**, *15*, 1059. [CrossRef] [PubMed]
11. Ohkubo, M.; Yamamura, M.; Uchiyama, H.; Nojima, T. Breathing clothes: Artworks using the hairlytop interface. In Proceedings of the 11th Conference on Advances in Computer Entertainment Technology, Madeira, Portugal, 11–14 November 2014; pp. 1–4.
12. Zięba, J.; Frydrysiak, M.; Błaszczyk, J. Textronic clothing with resistance textile sensor to monitoring frequency of human breathing. In Proceedings of the 2012 IEEE International Symposium on Medical Measurements and Applications Proceedings, Budapest, Hungary, 18–19 May 2012; pp. 1–6.
13. Chen, W.; McDuff, D. Deepphys: Video-based physiological measurement using convolutional attention networks. In Proceedings of the 15th European Conference on Computer Vision (ECCV), Munich, Germany, 8–14 September 2018; pp. 349–365.
14. Suriani, N.S.; Shahdan, N.S.; Sahar, N.M.; Taujuddin, N.S.A.M. Non-contact facial based vital sign estimation using convolutional neural network approach. *Int. J. Adv. Comput. Sci. Appl.* **2022**, *13*, 386–393. [CrossRef]
15. Goodfellow, I. *Deep Learning*; MIT Press: Cambridge, MA, USA, 2016.
16. Bengio, Y.; Simard, P.; Frasconi, P. Learning long-term dependencies with gradient descent is difficult. *IEEE Trans. Neural Netw.* **1994**, *5*, 157–166. [CrossRef]
17. Glorot, X.; Bengio, Y. Understanding the difficulty of training deep feedforward neural networks. In Proceedings of the Thirteenth International Conference on Artificial Intelligence and Statistics, Sardinia, Italy, 13–15 May 2010; pp. 249–256.
18. Srivastava, R.K.; Greff, K.; Schmidhuber, J. Highway networks. *arXiv* **2015**, arXiv:1505.00387.
19. He, K.; Zhang, X.; Ren, S.; Sun, J. Deep residual learning for image recognition. In Proceedings of the 2016 IEEE Conference on Computer Vision and Pattern Recognition (CVPR), Las Vegas, NV, USA, 27–30 June 2016; pp. 770–778.
20. Bello, I.; Fedus, W.; Du, X.; Cubuk, E.D.; Srinivas, A.; Lin, T.-Y.; Shlens, J.; Zoph, B. Revisiting resnets: Improved training and scaling strategies. *Adv. Neural Inf. Process. Syst.* **2021**, *34*, 22614–22627.
21. Mohsen, H.; El-Dahshan, E.-S.A.; El-Horbaty, E.-S.M.; Salem, A.-B.M. Classification using deep learning neural networks for brain tumors. *Future Comput. Inform. J.* **2018**, *3*, 68–71. [CrossRef]
22. Sadegh Ebrahimi, M.; Karkeh Abadi, H. Study of Residual Networks for Image Recognition. *arXiv* **2018**, arXiv:1805.00325.

23. Kim, J.-S.; Truong, T.; Kim, J. Development of embroidery-type sensor capable of detecting respiration using the capacitive method. *Polymers* **2023**, *15*, 503. [CrossRef]
24. Kim, J.; Kim, J. Classification of Breathing Signals According to Human Motions by Combining 1D Convolutional Neural Network and Embroidered Textile Sensor. *Sensors* **2023**, *23*, 5736. [CrossRef]
25. Kim, S.; Truong, T.; Jang, J.; Kim, J. The programmable design of large-area piezoresistive textile sensors using manufacturing by jacquard processing. *Polymers* **2022**, *15*, 78. [CrossRef]
26. *ISO 10993-5*; Biological evaluation of Medical Devices—Part 5: Tests for In Vitro Cytotoxicity. ISO: 2009. Available online: https://webdesk.jsa.or.jp/books/W11M0090/index/?bunsyo_id=ISO+10993-5:2009 (accessed on 21 January 2025).
27. Truong, T.; Kim, J.-S.; Kim, J. Design and optimization of embroidered antennas on textile using silver conductive thread for wearable applications. *Fibers Polym.* **2021**, *22*, 2900–2909. [CrossRef]
28. Pham, L.; Phan, H.; Palaniappan, R.; Mertins, A.; McLoughlin, I. CNN-MoE based framework for classification of respiratory anomalies and lung disease detection. *IEEE J. Biomed. Health Inform.* **2021**, *25*, 2938–2947. [CrossRef]
29. Seyfioğlu, M.S.; Özbayoğlu, A.M.; Gürbüz, S.Z. Deep convolutional autoencoder for radar-based classification of similar aided and unaided human activities. *IEEE Trans. Aerosp. Electron. Syst.* **2018**, *54*, 1709–1723. [CrossRef]
30. Raeis, H.; Kazemi, M.; Shirmohammadi, S. CAE-MAS: Convolutional Autoencoder Interference Cancellation for Multiperson Activity Sensing With FMCW Microwave Radar. *IEEE Trans. Instrum. Meas.* **2024**, *73*, 1–10. [CrossRef]
31. Brieva, J.; Ponce, H.; Moya-Albor, E. Non-contact breathing rate estimation using machine learning with an optimized architecture. *Mathematics* **2023**, *11*, 645. [CrossRef]
32. Chaichulee, S.; Villarroel, M.; Jorge, J.; Arteta, C.; McCormick, K.; Zisserman, A.; Tarassenko, L. Cardio-respiratory signal extraction from video camera data for continuous non-contact vital sign monitoring using deep learning. *Physiol. Meas.* **2019**, *40*, 115001. [CrossRef]
33. Hussain, F.; Abbas, S.G.; Husnain, M.; Fayyaz, U.U.; Shahzad, F.; Shah, G.A. IoT DoS and DDoS attack detection using ResNet. In Proceedings of the 2020 IEEE 23rd International Multitopic Conference (INMIC), Bahawalpur, Pakistan, 5–7 November 2020; pp. 1–6.


**Disclaimer/Publisher's Note:** The statements, opinions and data contained in all publications are solely those of the individual author(s) and contributor(s) and not of MDPI and/or the editor(s). MDPI and/or the editor(s) disclaim responsibility for any injury to people or property resulting from any ideas, methods, instructions or products referred to in the content.